The Astronomical Journal, 119:1130–1144, 2000 March

THE NEUTRAL HYDROGEN DISTRIBUTION IN MERGING GALAXIES: DIFFERENCES BETWEEN STELLAR AND GASEOUS TIDAL MORPHOLOGIES

J. E. Hibbard[1]
National Radio Astronomy Observatory,[2] 520 Edgemont Road, Charlottesville, VA 22903; jhibbard@nrao.edu
W. D. Vacca
Infrared Telescope Facility, Institute for Astronomy, 2680 Woodlawn Drive, Honolulu, HI 96822; vacca@ifa.hawaii.edu
and
M. S. Yun
National Radio Astronomy Observatory,[2] P.O. Box O, Socorro, NM 87801; myun@nrao.edu
Received 1999 September 22; accepted 1999 December 8

ABSTRACT

As part of several H I synthesis-mapping studies of merging galaxies, we have mapped the tidal gas in the three disk-disk merger systems Arp 157 (NGC 520), Arp 220, and Arp 299 (NGC 3690). These systems differ from the majority of the mergers mapped in H I in that their stellar and gaseous tidal features do not coincide. In particular, they exhibit large stellar tidal features with little if any accompanying neutral gas and large gas-rich tidal features with little if any accompanying starlight. On smaller scales, there are striking anticorrelations in which the gaseous and stellar tidal features appear to cross. We explore several possible causes for these differences, including dust obscuration, ram pressure stripping, and ionization effects. No single explanation can account for all of the observed differences. The fact that each of these systems shows evidence for a starburst-driven superwind expanding in the direction of the most striking anticorrelations leads us to suggest that the superwind is primarily responsible for the observed differences, either by sweeping the features clear of gas via ram pressure or by excavating a clear sightline toward the starburst and allowing UV photons to ionize regions of the tails. If this suggestion is correct, only systems hosting a galactic superwind and experiencing a high-inclination encounter geometry (such that tidal gas is lifted high above the starburst regions) should exhibit such extreme differences between their H I and optical tidal morphologies.

Key words: galaxies: individual (Arp 220, NGC 3690, NGC 520) — galaxies: interactions — galaxies: ISM — galaxies: peculiar — galaxies: starburst

1. INTRODUCTION

Nearly 30 years ago, Toomre & Toomre (1972) elegantly demonstrated that the tails and bridges emanating from many peculiar galaxies may arise kinematically from dynamically cold disk material torn off the outer regions of galaxies experiencing strong gravitational interactions. Early spectroscopic studies of gas within the tidal tails of merging galaxies provided observational support for this hypothesis by showing the tails to have the kinematics expected for a gravitational origin (e.g., Stockton 1974a, 1974b). H I mapping studies are particularly well suited to such studies, as the tidally ejected disk material is usually rich in neutral hydrogen and can be traced to very large distances from the merging systems (e.g., van der Hulst 1979; Simkin et al. 1987; Appleton, Davies, & Stephenson 1981, Appleton et al. 1987; Yun, Ho, & Lo 1994). Once mapped, the tidal kinematics can be used either alone to disentangle the approximate spin geometry of the encounter (Stockton 1974a, 1974b; Mihos, Bothun, & Richstone 1993; Hibbard & van Gorkom 1996, hereafter HvG96; Mihos & Bothun 1998) or in concert with detailed numerical models to constrain the full encounter geometry (e.g., Combes 1978; Combes et al. 1988; Yun 1992, 1997; Hibbard & Mihos 1995; Gardiner & Noguchi 1996).

However, not all systems can be easily explained by purely gravitational models such as those used by Toomre & Toomre (1972). For example, gravitational forces by themselves should not lead to differences between stellar and gaseous tidal components. Numerical models that include hydrodynamical effects do predict a decoupling of the dissipative gaseous and nondissipative stellar components (e.g., Noguchi 1988; Barnes & Hernquist 1991, 1996; Weil & Hernquist 1993; Mihos & Hernquist 1996; Appleton, Charmandaris, & Struck 1996; Struck 1997) but only in the inner regions or along bridges where gas orbits may physically intersect (see, e.g., Fig. 4 of Mihos & Hernquist 1996). Decoupling of the gaseous and stellar components within the tidal tails is not expected.

Nonetheless, differences between the optical and gaseous tidal morphologies have been observed. These differences can be subtle, with the peak optical and H I surface brightnesses simply displaced by a few kiloparsecs within the tails (e.g., NGC 4747: Wevers et al. 1984; NGC 2782: Smith 1994; NGC 7714/4: Smith, Struck, & Pogge 1997; Arp 295A, NGC 4676B, and the southern tail of NGC 520: Hibbard 1995, HvG96), or they can be extreme, with extensive H I tidal features apparently decoupled from, or even anticorrelated with, the optical tidal features. It is this latter category of objects that we wish to address in this paper. In

[1] Visiting Astronomer, Kitt Peak National Observatory, National Optical Astronomy Observatories, operated by the Association of Universities for Research in Astronomy, Inc. (AURA), under cooperative agreement with the National Science Foundation.

[2] The National Radio Astronomy Observatory is operated by Associated Universities, Inc., under cooperative agreement with the National Science Foundation.

particular, we address the morphology of the tidal gas and starlight in the merging systems NGC 520 (Arp 157), Arp 220, and Arp 299 (NGC 3690).

The three systems were observed as part of our ongoing studies on the tidal morphologies of optically and IR-selected mergers (Hibbard 1995; HvG96; Hibbard & Yun 1996, 2000). These studies involve moderate resolution ($\theta_{\rm FWHM} \sim 15''$) Very Large Array H I spectral-line mapping observations and deep optical B and R broadband imaging with large-format CCDs using the KPNO 0.9 m (NGC 520) and the University of Hawaii 88 inch telescopes. The H I and optical observations, reduction, and data products have been presented in Hibbard (1995) and HvG96 for NGC 520, in Hibbard & Yun (1999, hereafter HY99) for Arp 299, and in Yun & Hibbard (2000a; see also Hibbard & Yun 1996) for Arp 220. We refer the reader to these papers for details of the observations and data reduction. These systems are extremely disturbed, and we cannot hope to offer a full description of their peculiarities here. For more information we refer the reader to the above references.

2. OBSERVED STELLAR AND GASEOUS TIDAL MORPHOLOGIES

Figures 1, 2, and 3 show the optical and atomic gas morphologies of NGC 520, Arp 299, and Arp 220, respectively. For NGC 520 and Arp 220 only the inner regions are shown, to highlight the differences we wish to address. In each figure, the upper left panel shows a gray-scale representation of the optical morphology of the system with features of interest labeled. The upper right panel shows the H I distribution. Contours indicate the distribution of H I mapped at low-resolution ($\theta_{\rm FWHM} \sim 30''$), whereas the gray scales show the H I mapped at higher resolution ($\theta_{\rm FWHM} \sim 15''$). The former is sensitive to diffuse low column density ($N_{\rm H\,I}$) neutral hydrogen, while the latter delineates the distribution of the higher column density H I. The central region of each H I map appears to have a hole (*dashed contours*), which is due to H I absorption against the radio continuum associated with the diskwide starbursts taking place in each galaxy (see Condon et al. 1990). In the lower left panel, we again present the optical morphology in gray scales and the higher resolution H I distribution as contours. Finally, the lower right panel presents a smoothed, star-subtracted R-band image contoured on a gray-scale representation of the high-resolution H I map.

In the final panels of Figures 1, 2, and 3, dashed lines labeled "Slice" indicate the locations from which H I and optical intensity profiles have been extracted; these profiles are plotted in Figure 4. Arrows labeled "Superwind" indicate the position angle (P.A.) of Hα or soft X-ray plumes, believed to arise from a starburst-driven outflow or galactic superwind in each system. Such outflows are common in other IR-bright starbursts (e.g., Heckman, Armus, & Miley 1987, 1990, hereafter HAM90; Armus, Heckman, & Miley 1990; Lehnert & Heckman 1996) and are thought to arise when the mechanical energy from massive stars and supernovae in the central starburst is sufficient to drive the dense interstellar medium outward along the minor axis (e.g., Chevalier & Clegg 1985; Joseph & Wright 1985; Suchkov et al. 1994). Often, such starbursts are powerful enough to drive a freely expanding wind of hot plasma completely out of the galaxy ("blowout"; HAM90).

In the following subsections we briefly discuss what is known about the dynamic state of each system and describe the differences between the stellar and gaseous tidal morphologies. Throughout this paper distances and other physical properties are calculated assuming $H_0 = 75$ km s^{-1} Mpc^{-1}.

2.1. *NGC 520*

NGC 520 (Arp 157, UGC 966) is an intermediate-stage merger, with the two progenitor nuclei separated by 40″ (5.8 kpc for $D = 30$ Mpc, $1'' = 145$ pc) and embedded within a common luminous envelope (HvG96, and references therein; see Fig. 1*a*). There is a bright optical tidal tail stretching 24 kpc to the southeast (henceforth referred to as the S tail), which bends sharply eastward and connects to a broad optical plume.[3] This plume continues to the north and west for 60 kpc before it appears to connect to extended light surrounding the dwarf galaxy UGC 957 (outside the region plotted in Fig. 1*a*; see Stockton & Bertola 1980).

The primary nucleus (the easternmost nucleus in Fig. 1*a*) possesses a massive ($\sim 5 \times 10^9\ M_\odot$) 1 kpc scale rotating molecular gas disk (Sanders et al. 1988; Yun & Hibbard 2000b). An H I disk is kinematically centered on this molecular disk and extends to a radius of about 20 kpc (labeled "Inner Disk" in Fig. 1*b*). Beyond this there is an intermediate ring of H I with a mean radius of about 30 kpc (i.e., the material that contains the feature labeled "N Clump" in Fig. 1*b*) and a nearly complete outer ring of H I with a mean radius of 60 kpc, which extends smoothly through the dwarf galaxy[4] UCG 957 (only partially seen in Fig. 1*b*). There is a kinematic and morphological continuity between the molecular gas disk, the inner H I disk, and outer H I ring (Yun & Hibbard 2000b), which suggests that all of this material is associated with the primary nucleus.

The observations suggest that the NGC 520 interaction involved a prograde-retrograde or prograde–polar spin geometry. The linear morphology of the optical tail-to-plume system is typical of features produced by a disk experiencing a prograde encounter (i.e., the disk rotates in the same direction as the merging systems orbit each other). The disklike morphology and rotational kinematics of the large-scale H I and the lack of any aligned linear tidal features, on the other hand, are more typical of polar or retrograde encounter geometries (i.e., disk rotation either perpendicular to or opposite to the direction of orbital motion). Such encounters fail to raise significant tails (Toomre & Toomre 1972; Barnes 1988), and much of the disk material remains close to its original rotational plane.

Neither the intermediate nor the outer H I ring has an optical counterpart ($\mu_R > 27$ mag arcsec^{-2}). Despite smooth rotational kinematics, this outer H I has a very clumpy and irregular morphology, with notable gaps near the optical minor axis (labeled "NE gap" and "SW gap" in Fig. 1, *lower left panel*). This figure shows that the outer H I

[3] We follow the naming convention of Schombert, Wallin, & Struck-Marcell (1990) and refer to tidal features with flat intensity profiles as plumes and ones with Gaussian profiles as tails.

[4] The H I kinematics show that UGC 957 is kinematically associated with this outer gas ring, although it may lie slightly above or below it. Rudimentary numerical modeling has shown that it is unlikely that the UCG galaxy is responsible for the main optical features of the NGC 520 system (Stanford & Balcells 1991). It is unclear whether this system is an interloper or was recently assembled from the surrounding ring of gas.

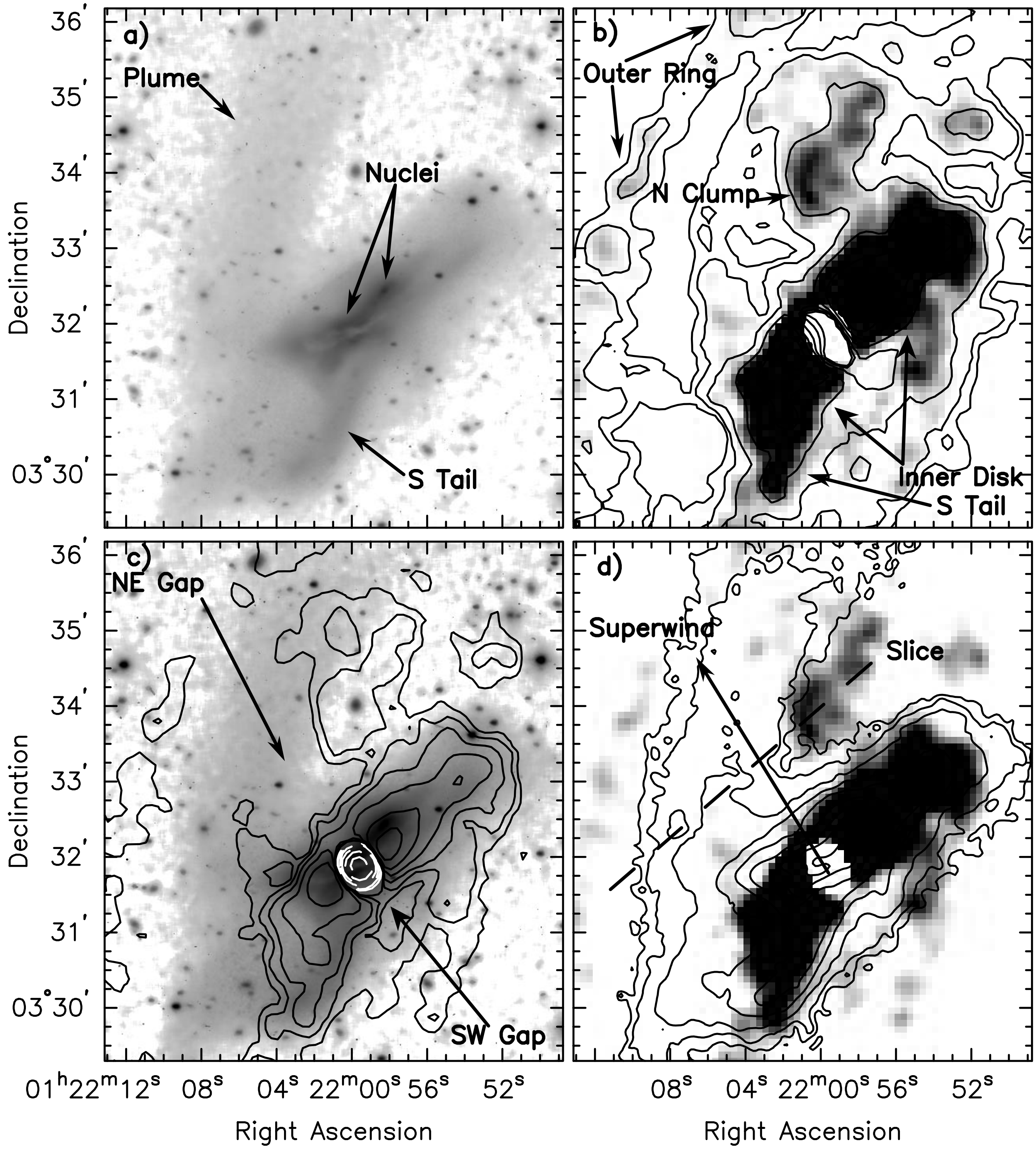

FIG. 1.—H I and optical morphology of NGC 520. *Upper left*: *R*-band image with labeled features. *Upper right*: Contour and gray-scale representation of the H I data. Contours indicate the distribution of H I mapped at low-resolution ($\theta_{FWHM} \sim 25''$), whereas gray scales show the H I mapped at higher resolution ($\theta_{FWHM} \sim 17''$). The lowest contour is drawn at a column density of 5×10^{19} cm^{-2}, with successive contours a factor of 2 higher. Gray scales range from 1×10^{20} cm^{-2} (*white*) to 4×10^{20} cm^{-2} (*black*). *Lower left*: Optical image in gray scales with contours from the high-resolution H I data superposed. The lowest contour is drawn at a column density of 1×10^{20} cm^{-2}, with successive contours a factor of 2 higher. *Lower right*: Contours from a star-subtracted *R*-band image (lowest contour 27 mag arcsec^{-2} and contour interval 1 mag arcsec^{-2}) on gray scales of the high-resolution H I data (from 1×10^{20} cm^{-2} to 4×10^{20} cm^{-2}). The dashed line labeled "Slice" indicates the locations of the intensity profiles plotted in Fig. 4*a*. The arrow labeled "Superwind" indicates the direction (but not the extent) of the putative expanding superwind.

and optical structures are anticorrelated, with the peak H I column densities (associated with the N clump) located to one side of the optical plume. In Figure 1, *lower right panel*, the H I clump appears to be bounded on three sides by the optical contours. In Figure 4*a*, we present an intensity profile at the location indicated by the dashed line in Figure 1, *lower right panel*, showing that the gas column density increases precisely where the optical light decreases.

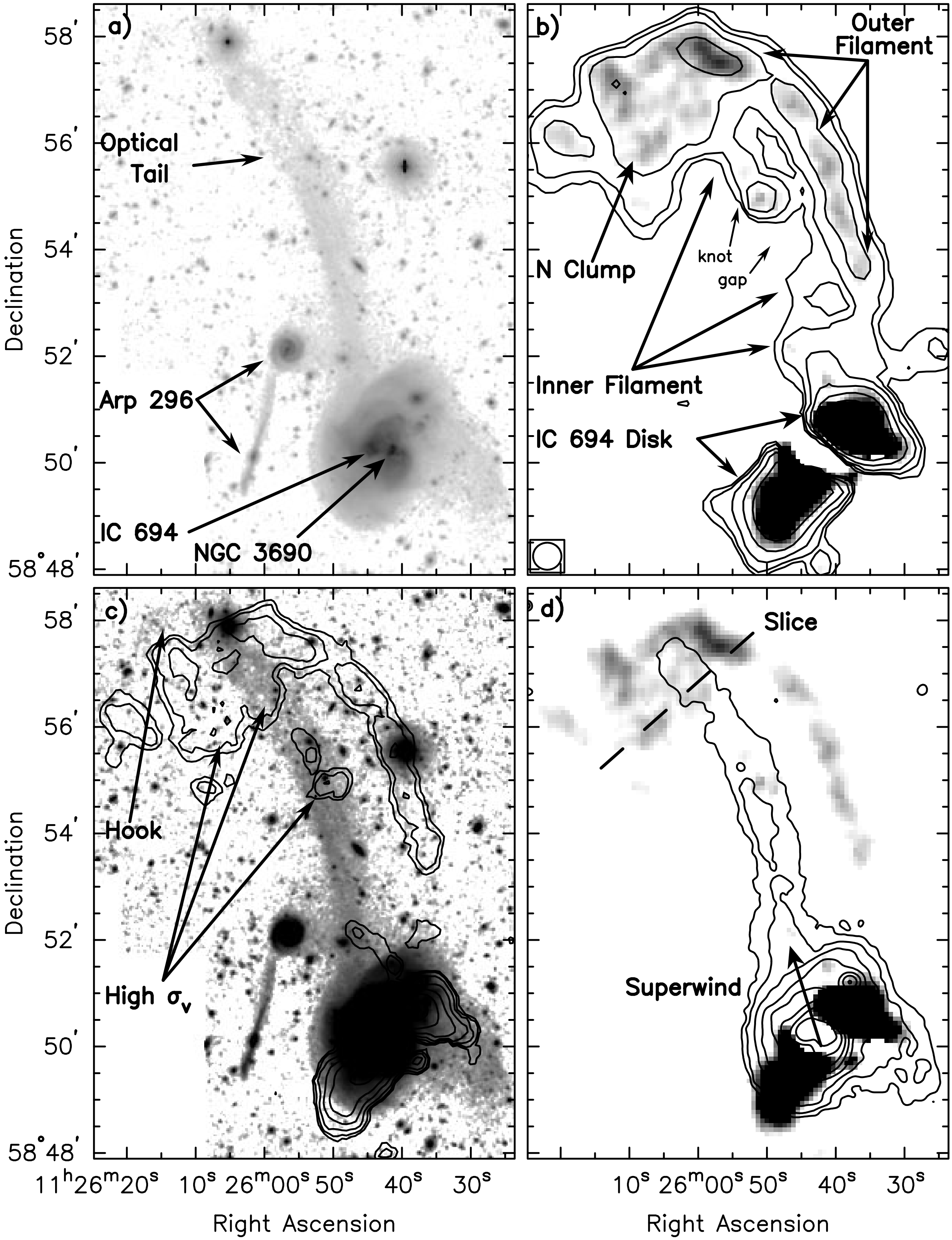

FIG. 2.—Same as Fig. 1, but for Arp 299. *Upper left and right*: For contours, at low-resolution, $\theta_{\rm FWHM} \sim 35''$, and for gray scales, at higher resolution, $\theta_{\rm FWHM} \sim 20''$. For the lowest contour, the column density is 2.5×10^{19} cm^{-2}; successive contours are a factor of 2 higher. Gray scales range from 1×10^{20} cm^{-2} (*white*) to 4×10^{20} cm^{-2} (*black*). *Lower left*: The lowest contour is drawn at a column density of 5×10^{19} cm^{-2}; successive contours are factor of 2 higher. *Lower right*: Lowest contour and contour interval as in Fig. 1. Intensity profiles are plotted in Fig. 4*b*.

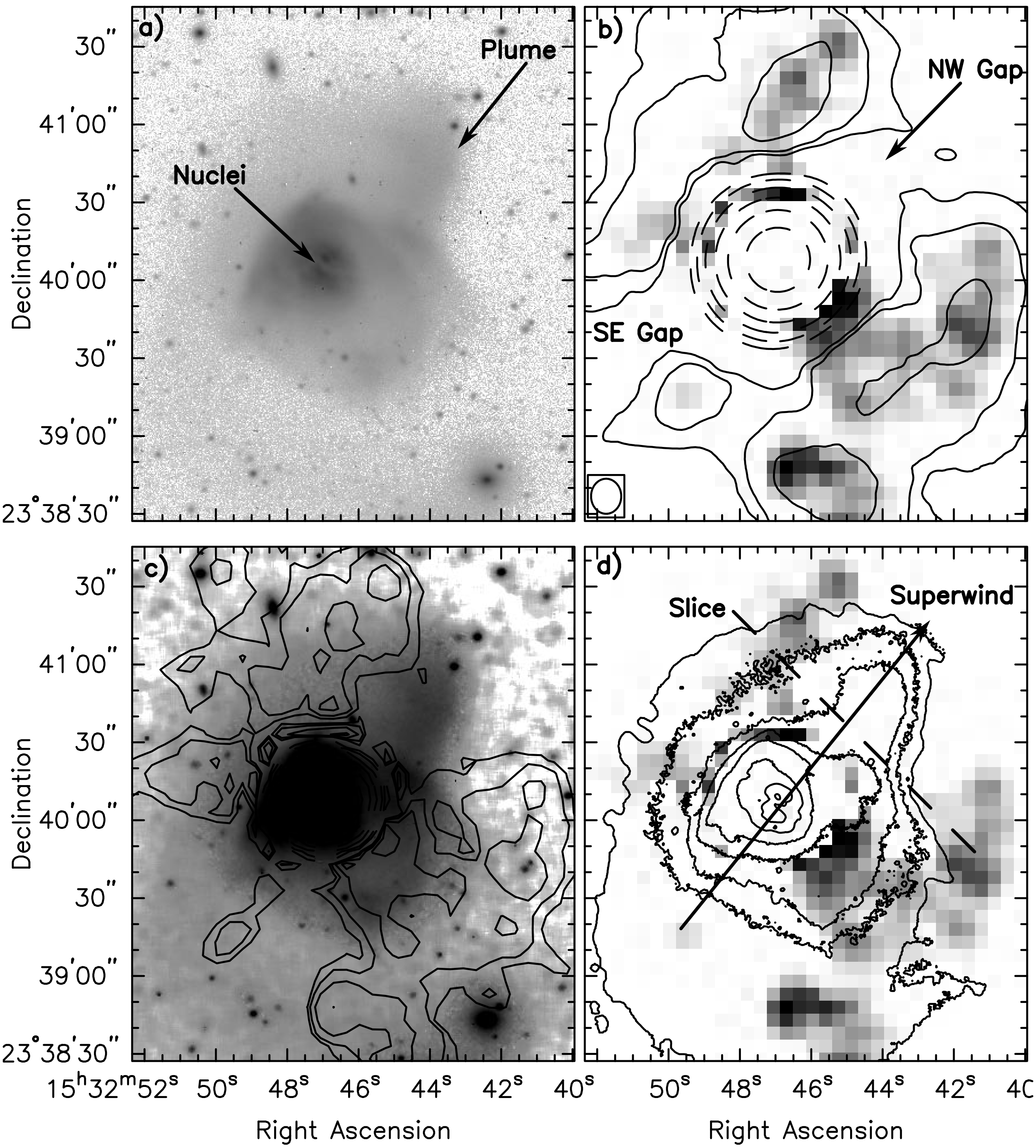

FIG. 3.—Same as Fig. 1, but for Arp 220. *Upper left and right*: For contours, at low-resolution, $\theta_{\rm FWHM} \sim 30''$, and for gray scales, at higher resolution, $\theta_{\rm FWHM} \sim 18''$. For the lowest contour, the column density is 5×10^{19} cm^{-2}; successive contours are a factor of 2 higher. Gray scales range from 1×10^{20} cm^{-2} (*white*) to 4×10^{20} cm^{-2} (*black*). *Lower left*: The lowest contour is drawn at a column density of 5×10^{19} cm^{-2}; successive contours are a factor of 2 higher. *Lower right*: Lowest contour is 26 mag arcsec^{-2} and contour interval is 1 mag arcsec^{-2}. Intensity profiles are plotted in Fig. 4*c*.

While the H I features exhibit a clear rotational kinematic signature, the well-defined edges and nearly linear structure of the optical plume suggest that its constituent stars are moving predominantly along the plume, rather than in the plane of the sky: any substantial differential rotation would increase the width of the plume and result in a more disklike morphology. We therefore conclude that the gas rings and optical plume are both morphologically and kinematically distinct entities. This suggests that the observed gas/star anticorrelation is either transient (and fortuitous) or actively maintained by some process.

A deep Hα image of NGC 520 shows plumes of ionized gas emerging both north and south along the minor axis and reaching a projected height of 3 kpc from the nucleus

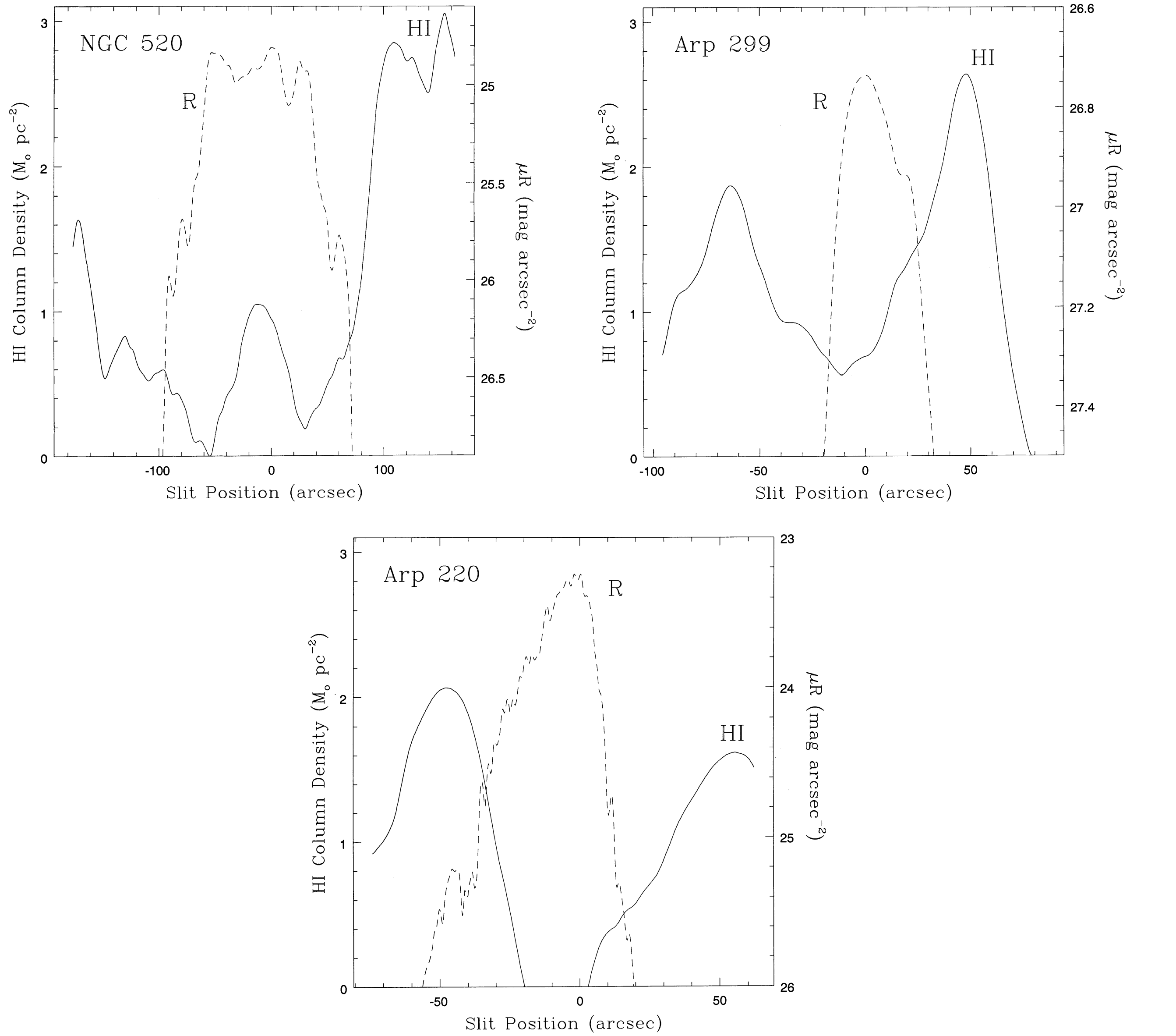

FIG. 4.—Intensity profiles of *R*-band surface brightness (μ_R) and H I column density (beam-averaged values measured from the low-resolution data) taken along the dashed lines in Figs. 1, *lower right panel*, 2*d*, and 3*d*. (*a*): NGC 520, across the northern plume. (*b*): Arp 299, across the tip of the northern tail. (*c*): Arp 220, across the northwestern plume. Gas column densities are measured in $M_\odot$ pc^{-2} (where 1 $M_\odot$ pc^{-2} = 1.25 × 10^{20} cm^{-2}) and optical surface brightnesses in mag arcsec^{-2}.

(HvG96). It has been suggested that this plume represents a starburst-driven outflow of ionized gas (HvG96; Norman et al. 1996). The position angle of this plume is indicated by an arrow in Figure 1 (*lower right panel*) (P.A. = 25°). This direction corresponds to the most dramatic H I/optical anti-correlations mentioned above, and in the following we suggest that this region of the optical tail actually lies directly in the path of the outflowing wind.

2.2. *Arp 299*

Arp 299 (NGC 3690/IC 694, UGC 6471/2, Mrk 171, VV 118) is also an intermediate-stage merger, with two disk systems (IC 694 to the east and NGC 3690 to the west; see Fig. 2*a*) in close contact but with their respective nuclei separated by 20″ (4.7 kpc for $D = 48$ Mpc, 1″ = 233 pc). A long, narrow, faint ($\mu_R \gtrsim 26$ mag arcsec^{-2}) tidal tail stretches to the north to a radius of about 125 kpc. H I imaging of this system by HY99 (see also Nordgren et al. 1997) shows a rotating gas-rich disk within the inner regions and a pair of parallel H I filaments extending to the north. From the H I morphology and kinematics, HY99 deduce that Arp 299 is the result of a prograde-retrograde or prograde-polar encounter between two late-type spirals, with the inner H I disk associated with the retrograde disk of IC 694 and the northern optical tail and tidal H I filaments ejected by the prograde disk of NGC 3690.

The parallel-filament or bifurcated morphology of the tidal H I is quite unlike that of the optical tail. The inner H I filament (so labeled in Fig. 2*b*) is of lower characteristic column density ($N_{\rm H\,I} \lesssim 8 \times 10^{19}$ cm^{-2}) and is associated with the low surface brightness stellar tail (Fig. 2*c*). The gas in this filament has a more irregular morphology than that in the outer filament (e.g., the "gap" and "knot" in Fig. 2*b*), and much of this material is detectable only after a substantial smoothing of the data (Fig. 2*b*). The outer filament is characterized by a higher H I column density ($N_{\rm H\,I} \sim 1.5 \times 10^{20}$ cm^{-2}) but has no optical counterpart ($\mu_R > 27.5$ mag arcsec^{-2}). This filament is displaced by approximately 20 kpc (in projection) to the west of the inner filament for much its length, after which the filaments merge together in a feature labeled the "N Clump" in Figure 2*b*. The parallel filaments have nearly identical kinematics along their entire lengths and join smoothly at the N clump. This implies that these features form a single physical structure.

Based on preliminary numerical simulations, HY99 suggest that a bifurcated morphology can arise quite naturally during tail formation. This occurs when the optically faint, gas-rich outer regions of the progenitor disk are projected adjacent to optically brighter regions coming from smaller initial radii (see also Mihos 2000).[5] However, this scenario does not explain why the inner filament, presumably drawn from optically bright but still gas-rich material within the optical disk of the progenitor, should lack accompanying H I.

As in NGC 520, there is an anticorrelation between the optical and gaseous column densities across the N clump, with the highest gas column densities (2–3 $\times 10^{20}$ cm^{-2}) located on either side of the optical tail. This is illustrated in Figure 4*b*, where we plot a profile along the position indicated by the dashed line in Figure 2*d*. The optical tail emerges above the N clump and appears to curve exactly around the northern edge of the N clump (labeled "hook" in Fig. 2*c*). Also labeled in Figure 2*c* are the three regions with anomalously high H I velocity dispersions noted by HY99 ($\sigma_{\rm H\,I} \sim 13$–20 km s^{-1} compared with $\sigma_{\rm H\,I} \sim 7$–10 km s^{-1} for the remainder of the tail; see Fig. 7*d* of HY99); we will refer to these regions in the discussion (§ 3.4.2).

Within the main body of Arp 299, vigorous star formation is taking place, with an inferred star formation rate (SFR) of 50 $M_\odot$ yr^{-1} (HAM90). Recent X-ray observations reported by Heckman et al. (1999) show evidence for hot gas emerging from the inner regions and reaching 25 kpc to the north, which the authors interpret as evidence for a hot, expanding superwind. The position angle of this feature (P.A. = 25°) is indicated by the arrow in Figure 2*d* and points toward the inner tidal filament and N clump.

2.3. *Arp 220*

Arp 220 (UGC 9913, IC 4453/4) is the prototypical ultraluminous infrared galaxy with $L_{8-100\,\mu\rm m} = 1.5 \times 10^{12}\ L_\odot$ (Soifer et al. 1984). It is an advanced merger system with two radio and infrared nuclei separated by 0″.9 (345 pc for $D = 79$ Mpc) and a bright optical plume extending 35 kpc to the northwest (Fig. 3*a*). Each of the two nuclei has its own compact molecular disk. The two nuclear disks are in turn embedded in one larger 1 kpc scale molecular gas disk (see Scoville, Yun, & Bryant 1997; Downes & Solomon 1998; Sakamoto et al. 1999, and references therein). The spin axis of the eastern nucleus is aligned with that of the kiloparsec-scale disk, while the western nucleus rotates in the opposite direction. These observations suggest that Arp 220 is the product of a prograde-retrograde merger of two gas-rich spiral galaxies (Scoville et al. 1997).

An irregular disklike distribution of neutral hydrogen extends over a 100 kpc diameter region surrounding the optical galaxy (Yun & Hibbard 2000a). The overall H I kinematics indicates that this material has a component of rotation in the same sense as that for the eastern nucleus and the molecular gas disk and opposite to the rotation of the western nucleus. This suggests that the H I disk and eastern nucleus originated from the retrograde progenitor, while the western nucleus and northwestern optical plume (Fig. 3*a*) arose from the prograde progenitor.

Because of the vigorous star formation occurring within Arp 220 (SFR = 340 $M_\odot$ yr^{-1}; HAM90), much of the H I within the optical body of the system is seen only in absorption against the bright radio continuum emission from the central starburst. Beyond this, the H I has high column densities ($N_{\rm H\,I} \sim 1.5 \times 10^{20}$ cm^{-2}), but only to the northeast and southwest. Most notably, there are local H I minima to the northwest and southeast (see gaps in Fig. 3*b*). Comparison of the H I map with the optical image (Fig. 3*c*) shows that the northwestern gap occurs exactly at the location of the optical tail. The relationship between the optical and H I surface brightness levels across this feature are illustrated by an intensity profile measured along the dashed line shown in Figure 3*d* and plotted in Figure 4*c*. As in NGC 520 and Arp 299, the gas column density increases precisely where the optical light from the tail begins to fall off. There is a similar H I gap to the southeast, but in this case there is no corresponding optical feature. At even larger radii, the H I is more diffuse ($N_{\rm H\,I} \sim 3 \times 10^{19}$ cm^{-2}) and has no optical counterpart down to $\mu_{\rm R} = 27$ mag arcsec^{-2}.

An X-ray image obtained with the *ROSAT* HRI camera (Heckman et al. 1996) reveals an extended central source that is elongated along P.A. = 135° (*arrows* in Fig. 3). A deep Hα + [N II] image of Arp 220 reveals ionized gas with a bright linear morphology at this same position angle (Heckman et al. 1987). The optical emission-line kinematics suggest a bipolar outflow (HAM90), and the physical properties of the warm and hot gas strongly support the superwind scenario for this emission (HAM90; Heckman et al. 1996). As in NGC 520 and Arp 299, the position angle of the putative expanding superwind is in the same direction as the H I minima, i.e., northwest and southeast.

3. DISCUSSION

Figures 1–4 provide evidence for both small- and large-scale differences in the distributions of the tidal gas and stars in these three systems. The small-scale differences are of the type illustrated in Figure 4, whereby the gas column density falls off just as the optical surface brightness increases at various edges of the tidal features.

In NGC 520 and Arp 220, the large-scale differences are between the outer H I rings and disks (which have no associated starlight) and the optical tails and plumes (which have no associated H I). Although these features are kinematically decoupled at present (with the gas rings and disks predominantly in rotation and the optical tails and plumes predominantly in expansion), it is possible that they had a common origin and have subsequently decoupled and evolved separately. In Arp 299, on the other hand, the H I filaments and optical tail have similar morphologies and continuous kinematics and are therefore part of the same kinematic structure. In this system we believe the bifurcated tidal morphology results from a progenitor with a warped

[5] To produce filaments as well separated as those found in Arp 299 HY99 suggests that the bifurcation is exacerbated by a preexisting gaseous warp in the progenitor disk.

gaseous disk (§ 2.2; HY99), and we seek to understand why the inner filament is gas-poor, given that its progenitor was obviously gas-rich.

In this section we investigate a number of possible explanations for these observations. In particular, we discuss the possible role played by differences in the initial radial distribution of the gas and stars (§ 3.1); dust obscuration (§ 3.2); kinematic decoupling of the gas due to collisions within the developing tidal tail (§ 3.3); ram pressure stripping of the gas, either by a halo or by a galactic scale wind (§ 3.4); and photoionization of the gas, either by the starburst or by local sources (§ 3.5).

3.1. *Differences in the Radial Distribution of Gas and Starlight*

In interacting systems, the H I is often more widely distributed than the optical light (see, e.g., the H I map of the M81 system by Yun et al. 1994; see also van der Hulst 1979; Appleton et al. 1981). These gas-rich extensions frequently have no associated starlight down to very faint limits (e.g., Simkin et al. 1987; HvG96). A natural explanation is that such features arise from the H I–rich but optically faint outer radii of the progenitor disks. The relatively short lifetimes of luminous stars and the larger velocity dispersions of less luminous stars, especially with respect to the gas, will further dilute the luminous content of this material, and the H I–to–light ratio of the resulting tidal features will increase with time (Hibbard et al. 1994). Gaseous tidal extensions with very little detectable starlight would seem to be the natural consequence. The outer H I rings in NGC 520 and Arp 220 and the gas-rich outer filament in Arp 299 are all likely to have arisen in this manner.

However, gas-rich outer disks cannot give rise to gas-poor optical structures, such as the optical plume in NGC 520, the optical tail in Arp 220, or the inner filament in Arp 299. Since these features presumably arise from optically brighter regions of the progenitor disks (regions that are characterized by H I column densities higher than that of the outer disks), one would have expected a priori that these features should also be gas-rich. It is possible that the disks that gave rise to the plumes in NGC 520 and Arp 220 were gas-poor at all radii. However, this would not account for the discontinuities in the outer gaseous features that project near these optical features (i.e., northeastern gap in NGC 520 and the northwestern gap in Arp 220). We therefore seek other explanations for these structures.

3.2. *Effects of Dust Obscuration*

The correspondence between rising gas column density and falling optical surface brightness (Fig. 4) suggests that dust associated with the cold gas may attenuate the optical light. To address this possibility, we calculate the expected extinction in the *R* band for a given column density of H I. We adopt the Milky Way dust-to-gas ratio determined by Bohlin, Savage, & Drake (1978; $N_{\rm H\,I}/E(B-V) = 4.8 \times 10^{21}$ cm^{-2} mag^{-1}), which is supported by direct imaging of the cold dust in the outer regions of eight disk galaxies (Alton et al. 1998). This is combined with the Galactic extinction law of O'Donnell (1994; $A_R/E(B-V) = 2.673$, from Table 6 of Schlegel, Finkbeiner, & Davis 1998) to yield an expected extinction in the *R* band of $A_R = N_{\rm H\,I}/(1.8 \times 10^{21} {\rm cm}^{-2})$ mag.

From Figure 4, the peak H I column densities on either side of the optical features are about 3×10^{20} cm^{-2}. The predicted extinction is therefore of order 0.2 mag in the *R* band. From Figure 4 we see that the mean light level drops by about 1.0 mag arcsec^{-2} for Arp 299 (from 26.5 mag arcsec^{-2} to below 27.5 mag arcsec^{-2}), about 1.5 mag arcsec^{-2} for NGC 520 (from 25 mag arcsec^{-2} to below 26.5 mag arcsec^{-2}), and by about 2.5 mag arcsec^{-2} for Arp 220 (from 23.5 mag arcsec^{-2} to below 26 mag arcsec^{-2}) along the extracted slices. To produce this amount of extinction, the tidal gas would have to have a dust-to-gas ratio that is 10 times that in the Milky Way.

The above analysis assumes that the measured neutral gas column density represents the total gas column density. However, the sharp drop in H I column density observed in many tidal features (HvG96; Hibbard & Yun 2000) suggests that the tidal gas may be highly ionized by the intergalactic UV field (see also the references in § 3.5). Since large dust grains should survive in the presence of this ionizing radiation, the opacity per atom of neutral hydrogen ($A_R/N_{\rm H\,I}$) should increase in regions of increasing ionization fraction. Observations of NGC 5018 (Hilker & Kissler-Patig 1996), in which blue globular clusters are absent in a region underlying an associated H I tidal stream, may support a high $A_R/N_{\rm H\,I}$ ratio for tidal gas. Nevertheless, the lack of obvious reddening of the $B-R$ colors along the slices in Arp 299 and NGC 520 (Hibbard 1995; HY99) argues against a much higher extinction in these regions.

We conclude that extinction might be important for shaping the morphology of the faintest optical features (e.g., the hook and the end of the optical tail of Arp 299, Fig. 2, which has μ_R near the detection limit of 28 mag arcsec^{-2}) but is insufficient to greatly affect the overall tidal morphology. However, an anomalously high tidal dust-to-gas ratio remains a possibility. This question could be resolved by the direct detection of cold dust in tidal tails with submillimeter imaging.

3.3. *Collisions within Developing Tidal Tails*

During the tail formation process, the leading edge of the tail is decelerated with respect to the center of mass of the progenitors, while the trailing edge is accelerated and the two edges move toward each other (see Fig. 3 in Toomre & Toomre 1972). Eventually, the two edges appear to cross, forming a caustic (Wallin 1990; Struck-Marcell 1990). In most cases, the caustics are simply due to projection effects. Only for low-inclination encounters will these crossings correspond to physical density enhancements, and numerical experiments suggest that in these cases the density will increase by factors of a few (Wallin 1990). It has been suggested that collisions experienced by the crossing tidal streams in such low-inclination encounters may lead to a separation between the dissipational (gas) and nondissipational (stellar) tidal components (Wevers et al. 1984; Smith et al. 1997).

The present data do not allow us to directly address this question, since the kinematic decoupling presumably took place long ago. However, several arguments lead us to suspect that this collisional process is not important in tidal tails: (1) large-scale decoupling between the stellar and gaseous tidal morphologies is not seen in many systems known to have experienced low-inclination encounters (e.g., NGC 4038/9, "The Antennae," in Hibbard, van der Hulst, & Barnes 2000; NGC 7252, "Atoms for Peace," Hibbard et al. 1994; NGC 4676, "The Mice," HvG96); (2) the broad, plumelike morphologies of the optical features in Arp 220 and NGC 520 suggest rather inclined encounters (§§ 2.1 and 2.3), in which case widespread collisions are not expected; and (3) the parallel filaments in the Arp 299 tail have identical kinematics, whereas one would expect kinematic differences between the stripped and unstripped material.

Therefore, while gaseous collisions and dissipation might result in differences between gas and stars during tidal development (particularly along tidal bridges, where the gas streamlines are converging; e.g., Struck 1997; NGC 7714/5, Smith et al. 1997; Arp 295, HvG96), we believe that they are not likely to lead to a widespread decoupling in the outer regions.

3.4. *Ram Pressure Stripping*

If the tidal features pass through a diffuse warm or hot medium or if such a medium passes through the tidal features, it is possible that the tidal gas exchanges energy and momentum with this medium via collisions. Such effects have been proposed to explain the stripping of the cool interstellar medium from spiral galaxies as they move through the hot intergalactic medium (IGM) in clusters (Gunn & Gott 1972) and is referred to as ram pressure stripping (RPS). Tidal features should be relatively easily stripped, as they lack the natural restoring forces present in disk galaxies, except possibly at a small number of self-gravitating regions. In this case, the momentum imparted by ram pressure is simply added to or subtracted from the momentum of the gaseous tidal features, and a separation of stellar and gaseous components might be expected.

In the next two subsections, we investigate two possible sources for ram pressure: an extended halo associated with the progenitors (§ 3.4.1) and an expanding starburst-driven superwind (§ 3.4.2).

3.4.1. *RPS from Extended Halo Gas*

Our own galaxy is known to have an extended halo of hot gas (Pietz et al. 1998). The existence of similar halos around external galaxies has been inferred from observations of absorption-line systems around bright galaxies (e.g., Lanzetta et al. 1995). These halos may have sufficient density to strip any low column density gas moving through them. Several investigators have suggested that such stripping is responsible for removing gas from the Magellanic Clouds as they orbit through the Galaxy's halo, producing the purely gaseous Magellanic Stream (e.g., Meurer, Bicknell, & Gingold 1985; Sofue 1994; Moore & Davis 1994). Sofue & Wakamatsu (1993) and Sofue (1994) specifically stress that stripping by galaxy halos should also play an important role in the evolution of H I tidal tails.

The tidal features in each of our systems have H I column densities and velocities similar to those assumed in the numerical models of Sofue (1994) and Moore & Davis (1994), which resulted in rather extreme stripping of the H I clouds. Although this may seem to provide an immediate explanation for our observations of gas/star displacements, we point out that these column densities and velocities are typical of all of the tails thus far imaged in H I, the great majority of which do not show the extreme displacements we describe here. There is no reason to believe that the halo properties of NGC 520, Arp 299, and Arp 220 are any different from, or that the encounters were any more violent than, similar mergers that do not exhibit such dramatic displacements (e.g., NGC 4038/9, NGC 7252, and NGC 4676: HvG96; NGC 3628: Dahlem et al. 1996; NGC 2623, NGC 1614, and Mrk 273: Hibbard & Yun 2000; NGC 3256: English et al. 2000). In fact, in light of the stripping simulations mentioned above, one wonders why such displacements are not more common.

A possible solution to this puzzle is suggested by the results of numerical simulations of major mergers. In these simulations, the material distributed throughout the halos of the progenitors is tidally distended along the tails, forming a broad sheath around them (see e.g., the video accompanying Barnes 1992). This sheath has kinematics similar to the colder tail material, resulting in much lower relative velocities than if the tail were moving through a static halo, thereby greatly reducing any relative ram pressure force.

In summary, while halo stripping might be effective for discrete systems moving through a static halo (such as the LMC/SMC through the halo of the Galaxy, or disks through a hot cluster IGM), the lack of widespread H I/optical decoupling in mergers suggests that it is not very effective for removing gas from tidal tails, and it does not appear to be a suitable explanation of the present observations.

3.4.2. *RPS from Expanding Superwind*

The three systems under discussion host massive nuclear starbursts with associated powerful outflows or "superwinds." Optical emission lines and/or X-ray emission reveal that the observed outflows extend for tens of kiloparseconds from the nuclear regions. Theoretical calculations suggest that the observed gas plumes represent just the hottest, densest regions of a much more extensive, lower density medium (Wang 1995). In each of these three systems, the most extreme gaps in the H I distribution appear along the inferred direction of the expanding hot superwinds (Figs. 1*d*, 2*d*, and 3*d*). A very similar anti-correlation between an outflowing wind and tidally disrupted H I has been observed in the M82 system (Yun et al. 1993; Strickland, Ponman, & Stevens 1997; Shopbell & Bland-Hawthorn 1998), the NGC 4631 system (Weliachew, Sancisi, & Guelin 1978; Donahue, Aldering, & Stocke 1995; Wang et al. 1995; Vogler & Pietsch 1996), and possibly the NGC 3073/9 system (Irwin et al. 1987; Filippenko & Sargent 1992). It has been suggested that this anti-correlation is due to an interaction between the blown-out gas of the superwind and the cold gaseous tidal debris, either as the wind expands outward into the debris or as the tidal debris passes through the wind (Chevalier & Clegg 1985; Heckman et al. 1987; and references above).

Figure 5 presents the suggested geometry for the case of Arp 299. This figure is constructed from our preliminary efforts to model the northern tail of Arp 299 using *N*-body simulations similar to those presented in Hibbard & Mihos (1995; i.e., no hydrodynamical effects are included). We found that we could not match the morphology and kinematics of both filaments simultaneously but could match either one separately. Figure 5 presents the results of combining these two solutions. In this sense, this figure is not a self-consistent fit to the data but simply a cartoon that illustrates the proposed relative placement of the tidal tail and the expanding wind. In this figure, the wind opening angle is illustrated by the cone; the gas-rich regions of the tails are represented by dark and light gray circles; and the gas-poor regions of the tails are represented by white circles. The

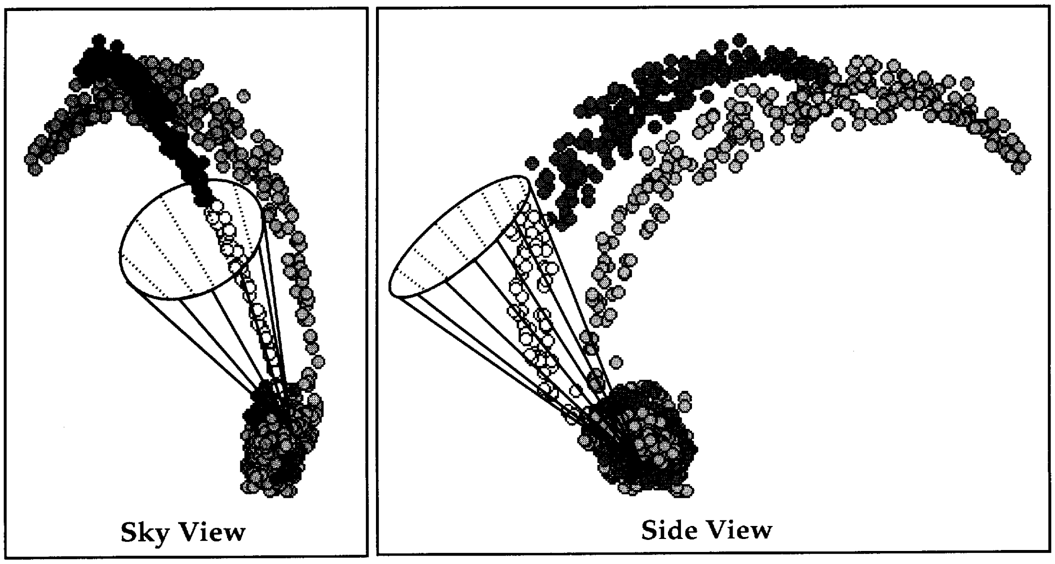

FIG. 5.—Proposed relative placement of the tidal tail and the expanding wind or ionization cone for Arp 299, showing the purely gaseous tidal filament (*light gray circles*) and the optical tidal filament, with regions of the optical tail that have accompanying H I (*dark gray circles*) and regions that have been cleared of H I (*white circles*; see Fig. 2). The suggested geometry of the superwind bubble (cf. § 3.4.2) or ionization cone (cf. § 3.5.1) is indicated by the cone, which has been drawn to encompass the white circles in the optical filament. The restricted opening angle of such a cone may intersect only a portion of the ribbonlike tail.

figure illustrates how the restricted opening angle of such a wind (or of an ionization cone; cf. § 3.5.1) may intersect only a portion of the ribbonlike tail.

Here we estimate whether ram pressure stripping by the nuclear superwind can exert sufficient pressure on gas at the large distances typical of tidal tails. We use equation (5) from Heckman, Lehnert, & Armus (1993; see also Chevalier & Clegg 1985) to calculate the expected ram pressure ($P_{\rm RPS}$) of the superwind far from the starburst as a function of its bolometric luminosity ($L_{\rm bol}$):

$$P_{\rm RPS}(r) = 4 \times 10^{-10}\ {\rm dyn\ cm^{-2}} \left(\frac{L_{\rm bol}}{10^{11}\ L_\odot}\right)\left(\frac{1\ {\rm kpc}}{r}\right)^2 . \quad (1)$$

This equation has been shown to fit the pressure profile derived from X-ray and optical emission-line data of Arp 299 (Heckman et al. 1999). It should provide a lower limit to the ram pressure, since it assumes that the wind expands spherically, while observations suggest that the winds are limited in solid angle.

This pressure can be compared with the pressure of the ambient medium in the tidal tail (P_t), given by the energy per unit volume:

$$P_t = C \rho_{\rm gas} \sigma_{\rm gas}^2 , \quad (2)$$

where C is a constant, $\rho_{\rm gas}$ is the mass density of the gas, and $\sigma_{\rm gas}$ is the velocity dispersion of the gas. For an equation of state of the form $P \sim \rho^\gamma$, the constant C is equal to $\gamma^{-1} = \frac{3}{5}$, and $\sigma_{\rm gas}$ corresponds to gas sound speed, while for a self-gravitating cloud, $C = 3/2$ and $\sigma_{\rm gas}$ is the one-dimensional velocity dispersion of the cloud. In both cases, we assume that the observed line-of-sight velocity dispersion of the H I is a suitable measure of $\sigma_{\rm gas}$.

The mass density of the tidal gas is given by $\rho_{\rm gas} = 1.36 m_{\rm H} n_{\rm H\,I}$, where the numerical constant accounts for the presence of He, $m_{\rm H}$ is the mass of a hydrogen atom, and $n_{\rm H\,I}$ is the number density of atomic hydrogen. If we assume the gas is uniformly distributed[6] with a column density $N_{\rm H\,I}$ along a length dL, we have $n_{\rm H\,I} = 6.5 \times 10^{-3}\ {\rm cm^{-3}}\ [N_{\rm H\,I}/(2 \times 10^{20}\ {\rm cm^{-2}})](10\ {\rm kpc}/dL)$, where the fiducial values are typical of tidal features (HvG96; Hibbard & Yun 2000). We rewrite equation (2) in terms of the observables:

$$P_t = 2 \times 10^{-14}\ {\rm dyn\ cm^{-2}} \left(\frac{C}{1.5}\right) \times \left(\frac{N_{\rm H\,I}}{2 \times 10^{20}\ {\rm cm^{-2}}}\right)\left(\frac{10\ {\rm kpc}}{dL}\right)\left(\frac{\sigma_{\rm H\,I}}{10\ {\rm km\ s^{-1}}}\right)^2 . \quad (3)$$

The maximum radius out to which we expect material to be stripped ($R_{\rm RPS}$) is then given by the requirement that $P_{\rm RPS}(r) = P_t(r)$ at $r = R_{\rm RPS}$. We replace $L_{\rm bol}$ in equation (1) by the IR luminosity ($L_{\rm IR}$), under the assumption that the IR luminosity arises from reprocessed UV photons from the starburst (Lonsdale, Persson, & Matthews 1984; Joseph & Wright 1985).[7] The very high IR luminosities of these systems ($L_{\rm IR}/L_B > 10$) make it likely that this is indeed the case, and we are probably making an error of $\lesssim 10\%$ (e.g., Heckman et al. 1993). Equating equations (1) and (3) we find

$$R_{\rm RPS} = 140\ {\rm kpc} \left(\frac{1.5}{C}\right)^{1/2}\left(\frac{L_{\rm IR}}{10^{11}\ L_\odot}\right)^{1/2} \times \left(\frac{2 \times 10^{20}\ {\rm cm^{-2}}}{N_{\rm H\,I}}\right)^{1/2}\left(\frac{dL}{10\ {\rm kpc}}\right)^{1/2}\left(\frac{10\ {\rm km\ s^{-1}}}{\sigma_{\rm H\,I}}\right) . \quad (4)$$

In Table 1 we provide estimates of $R_{\rm RPS}$ for the systems considered here. In calculating $R_{\rm RPS}$, we made the very conservative assumption that the values of $N_{\rm H\,I}$ and $\sigma_{\rm H\,I}$ for the stripped gas are equal to the maximum values found within

[6] Clearly the results will be very different if the tidal gas is mainly in dense clouds, a point that can be tested with higher-resolution VLA observations. For now we calculate the ram pressure effect on the diffuse gas.

[7] This assumes that the IR luminosity is not enhanced by the presence of an active galactic nucleus (AGN). There is no evidence for an energetically important AGN in any of these three systems.

TABLE 1

EFFECTS OF RAM PRESSURE AND IONIZATION ON TIDAL MATERIAL

Parameter	NGC 520	Arp 299	Arp 220	Notes
V_{hel} (km s^{-1})	2260	3080	5400	
D (Mpc)	30	48	79	1
L_{IR} ($L_\odot$)	7.6×10^{10}	8.1×10^{11}	1.5×10^{12}	2
$N_{H\,I}$, max (cm^{-2})	5×10^{20}	4×10^{20}	4×10^{20}	3
$\sigma_{H\,I}$, max (km s^{-1})	16	20	40	3
r (kpc)	25	70	30	4
R_{RPS} (kpc)	50	140	95	5
R_{ion} (kpc)	25	95	130	6

NOTES.—(1) Adopting the distances from Sanders, Scoville, & Soifer 1991, which assumes $H_0 = 75$ km s^{-1} Mpc^{-1}, and the Virgocentric flow model of Aaronson et al. 1982. (2) 8–1000 μm luminosity, from Sanders et al. 1991. (3) Maximum values of gas column density and line-of-sight velocity dispersion observed in the tidal features, taken from HvG96 (NGC 520), HY99 (Arp 299), and Yun & Hibbard 2000a (Arp 220). (4) The projected radius of "missing" H I. (5) Calculated from eq. (4), assuming the values given in this table and $dL = 10$ kpc. (6) Calculated from eq. (6), assuming the values given in this table and $f_{esc}(\Omega_w) = 0.1$ and $dL = 10$ kpc.

the tidal tails (see Table 1). The results of these calculations indicate that, in all cases, R_{RPS} is larger than the radii of the observed gaps in the tidal H I distributions. Therefore, in principle, the wind should be able to strip the gas from any tidal material in its path.

The above derivation assumes that the tidal gas is at rest with respect to the wind. It can be easily generalized to the case of a wind impacting an expanding tidal feature by reducing the wind ram pressure by a factor $[(V_w - V_t)/V_w]^2$, where w is wind and t is tidal. For NGC 520 and Arp 220, the tidal gas is primarily in rotation (i.e., moves perpendicular to superwind), so we expect the gas to feel the full ram pressure given above. For Arp 299, Heckman et al. (1999) find $V_w = 800$ km s^{-1}, and we estimate a maximum $V_t = 240$ km s^{-1} (HY99). Therefore, the ram pressure could be reduced by 50%, reducing R_{RPS} by 70% from that listed in Table 1, i.e., $R_{RPS} \sim 100$ kpc for Arp 299. This is still large enough to reach to the region of the N clump in Figure 2. The regions of high H I velocity dispersion indicated in Figure 2*c* may be due to the influence of such a wind. We note that these regions occur on the side of the H I features that face the starburst region. However, no such kinematic signatures are visible in the gas near the wind axis in NGC 520 or Arp 220.

The lack of gaseous/stellar displacements in the tidal tails of many superwind systems might seem to provide a strong argument against the scenario outlined above. However, two conditions are needed to produce wind-displaced tidal features: the starburst must be of sufficient energy and duration to achieve blowout and the tidal H I must intersect the path of the expanding wind material. The second condition is not met for the blowout systems NGC 4676, NGC 3628, NGC 2623, NGC 1614, and NGC 3256 (references given in § 3.4.1). In these systems, the tidal tails appear to lie at large angles with respect to the blowout axis, and their tidal tails should not intersect the wind. Both conditions are met for M82 and NGC 4631, which both show extreme H I/optical displacements. For these two systems, the high-latitude H I appears to be accreted from nearby disturbed companions (M81 and NGC 4656, respectively; Yun, Ho, & Lo 1993; Weliachew et al. 1978), while for the three major mergers under study here the H I appears to intercept the path of the wind as a result of a highly inclined encounter geometry. A high-inclination encounter geometry is therefore a prerequisite for such displaced morphologies, and the host of the superwind should be the disk with a retrograde or polar-spin geometry.

Nevertheless, ram pressure stripping cannot provide a complete explanation of the observations. Since the stars are unaffected by the wind, it would be an unusual coincidence for the edges of the optical plumes to correspond with the edge of the cold gas, which is presently being ablated. Nor does it seem likely that the wind could be sufficiently collimated to "bore" into the northern H I clump in Arp 299 just where the optical tail appears projected on it. Therefore a second process is still needed to explain the small-scale anticorrelations. In conclusion, the expanding wind *should* affect any tidal H I in its path; however, this effect alone cannot explain all the details of the observations.

3.5. *Photoionization*

Disk galaxies are known to exhibit a precipitous drop in neutral hydrogen column density beyond column densities of a few times 10^{19} cm^{-2} (Corbelli, Schneider, & Salpeter 1989; van Gorkom 1993; Hoffman et al. 1993). This drop has been attributed to a rapid change in the ionization fraction of the gas due to influence of the intergalactic UV field (Maloney 1993; Corbelli & Salpeter 1993; Dove & Shull 1994; see also Felten & Bergeron 1969; Hill 1974), rather than a change in the total column density of H.

Tidal tails are assembled from the outermost regions of disk galaxies. Since this material is redistributed over a much larger area than it formerly occupied, its surface brightness must decrease accordingly. Therefore, if the progenitors were typical spirals, with H I disks extending to column densities of a few times 10^{19} cm^{-2}, then the resulting tidal tail *must* have gas at much lower column densities. However, tidal tails exhibit a similar edge in their column density distribution *at a similar column density* (HvG96; Hibbard & Yun 2000). This is one of the most compelling pieces of evidence for an abrupt change in the phase of the gas at low H I column density. The outer tails mapped in H I should therefore be the proverbial "tip of the iceberg" of a lower column density, mostly ionized medium. With the tidal gas in this very diffuse state, fluctuations in the incident ionizing flux might be expected to produce accompanying fluctuations in the neutral gas fraction.

Given these considerations, we examine the possibility that the total hydrogen column density does not change in the regions illustrated in Figures 1–4, but that the neutral fraction does, i.e., that the gas in the regions under study has a higher ionization fraction than adjacent regions. The intergalactic UV field should be isotropic and would not selectively ionize certain regions of the tails. Here we examine the possibility of two nonisotropic sources of ionizing flux: (1) leakage of UV flux from the circumnuclear starburst and (2) ionization by late-B stars and white dwarfs associated with the evolved stellar tidal population.

Our procedure is to compare the expected ionizing flux density shortward of 912 Å to the expected surface recombination rate of the gas. We assume that in the area of interest the gas is at a temperature of about 10^4 K, for which a case B recombination coefficient of $\alpha_B = 2.6 \times 10^{-13}$ cm^3 s^{-1} is appropriate (Spitzer 1956). We assume that the hydrogen is almost completely ionized, so $n_e \approx n_{\rm H}$. We further assume that the density of ionized gas is the same as the density of the neutral gas in the adjacent regions, $n_{\rm H} \approx n_{\rm H\,I}$, where $n_{\rm H\,I}$ is calculated as above ($n_{\rm H} \sim N_{\rm H\,I}/dL$; § 3.4.2). The detailed ionization state will depend sensitively on the clumpiness of the gas, but a full treatment of this problem is beyond the scope of this paper. Here we wish to investigate whether these processes are in principle able to create effects similar to those observed.

3.5.1. *Photoionization by the Starburst*

Here we consider the case that the superwind does not affect the tidal gas by a direct interaction but influences it by providing a direct path from the tidal regions to the starburst, free of dust and dense gas (see also Fig. 5). Through these holes, ionizing photons from the young, hot stars stream out of the nuclear regions and are quickly absorbed by the first neutral atoms they encounter. Following Felton & Bergeron (1969; see also Maloney 1993), we solve the equation

$$n_{\rm H\,I}^2 \alpha_B \, dL = I = \frac{1}{4\pi r^2} \int_{h\nu = 13.6 \text{ eV}}^{\infty} \frac{L_\nu}{h\nu} d\nu \, . \quad (5)$$

The right-hand side of this equation represents the total ionizing radiation escaping the starburst region along a direction that has been cleared of obscuring material by the superwind. We express this in terms of the total ionizing flux of a completely unobscured starburst of a given bolometric luminosity $L_{\rm bol}$ by introducing the factor $f_{\rm esc}(\Omega_w)$, where w is wind, to account for the fact that only a fraction of the photons emitted into a solid angle Ω_w find their way out of the starburst region.[8] The expected ionizing flux for a starburst of a given bolometric luminosity $L_{\rm bol}$ is calculated from the population synthesis models of Bruzual & Charlot (1993; private communication 1995), assuming continuous star formation with a duration longer than 10 Myr (long enough for the burst to achieve blowout), a Salpeter initial mass function (IMF) with lower mass $M_l = 0.1\ M_\odot$ and upper mass $M_u = 125\ M_\odot$, and solar metallicity. This yields[9] $I = f_{\rm esc}(\Omega_w)(1.83 \times 10^{54}/4\pi r^2)$ photons s^{-1} $(L_{\rm bol}/10^{11}\ L_\odot)$. Again making the standard assumption that most of the starburst luminosity is emitted in the far-infrared (i.e., $L_{\rm bol} = L_{\rm IR}$; cf. § 3.4.2), we rearrange equation (5) to solve for the radius, $R_{\rm ion}$, out to which the starburst is expected to ionize a given column density of H I of thickness dL:

$$R_{\rm ion} = 66 \text{ kpc} \left[\frac{f_{\rm esc}(\Omega_w)}{0.10}\right]^{1/2} \left(\frac{L_{\rm IR}}{10^{11}\ L_\odot}\right)^{1/2} \times \left(\frac{2 \times 10^{20} \text{ cm}^{-2}}{N_{\rm H\,I}}\right)\left(\frac{dL}{10 \text{ kpc}}\right)^{1/2} . \quad (6)$$

Resulting values for $R_{\rm ion}$ are listed in Table 1. For this computation, we have adopted a value of 10% for $f_{\rm esc}(\Omega_w)$. This is equal to the total fraction of ionizing photons, $f_{\rm esc}$, escaping from a normal disk galaxy as calculated by Dove, Shull, & Ferrara (2000). Even higher values of $f_{\rm esc}$ are expected in starburst systems (Dove et al. 2000). Since we stipulate that a higher fraction of ionizing photons escape along sightlines above the blowout regions than are emitted along other directions, it follows that $f_{\rm esc}(\Omega_w) > f_{\rm esc}$, and as a result the values of $R_{\rm ion}$ calculated in Table 1 should be conservative estimates.

Table 1 shows that under these simplified conditions $R_{\rm ion}$ is of the order of, or larger than, the tidal radii of interest. We therefore conclude that the starburst seems quite capable of ionizing tidal H I, if indeed there is an unobstructed path from the starburst to the tidal regions. This might explain the lack of H I along the wind axis in NGC 520 and Arp 220 and the absence of H I along the optical tidal tail in Arp 299.

This process is especially attractive, since it possibly explains the lack of H I at the bases of otherwise gas-rich tidal tails in NGC 7252 (Hibbard et al. 1994), Arp 105 (Duc et al. 1997), and NGC 4039 (Hibbard et al. 2000). These systems do *not* show evidence for expanding superwinds, which rules out the possibility that RPS is playing a role. And each of these systems possesses a level of star formation that, according to equation (6), is capable of ionizing gas out to the necessary radii.

However, photoionization by the central starburst does not seem capable of explaining all of the observations. As with the wind hypothesis above, it would be an unusual coincidence for the edges of the optical plumes to correspond to the edge of the ionization cone. Therefore a second process is still needed to explain the small-scale anticorrelations.

3.5.2. *Photoionization by the Optical Tails*

The fact that the H I column density falls off just as the optical surface brightness increases at the edges of various tidal features (Fig. 4) leads us to suspect that there may be local sources of ionization within the stellar features themselves. For NGC 520 and Arp 220, we believe the outer H I is in a disk structure that is intersected by the tidal stellar

[8] It is important to differentiate $f_{\rm esc}$, the total fraction of ionized photons emerging from a starburst, and $f_{\rm esc}(\Omega_w)$, the fraction emerging along a particular sightline. $f_{\rm esc}$ is the total angle-averaged fraction, i.e., $f_{\rm esc}$ is the integral of $f_{\rm esc}\, d\Omega$ over all solid angles, while $f_{\rm esc}(\Omega_w)$ is the integral over a solid angle cleared by the wind. Most studies in the literature quote values for $f_{\rm esc}$.

[9] With similar assumptions, the "Starburst99" models of Leitherer et al. (1999) give approximately the same numerical coefficient.

plumes, and we wish to investigate whether ionization by evolved sources within the stellar plumes, such as late-B stars and white dwarfs, could be responsible for decreasing the neutral fraction of the diffuse outer H I. For Arp 299 the geometry is more complicated, and we refer the reader to Figure 5. Here we suggest that part of the purely gaseous tidal filament (the light gray filament in Fig. 5) is ionized by evolved sources near the end of the stellar tail (the dark gray filament in Fig. 5, especially those regions nearest the gas-rich filament in the right-hand panel of this figure).

As in the previous section, we balance the surface recombination rate with the expected ionizing flux density (eq. [5]). In this case, we calculate the ionizing flux density for an evolved population of stars of a given R-band luminosity density (Σ_R, in $L_\odot$ pc^{-2}).

To approximate the stellar populations in the tidal tails, we assume that the tails arise from the outer edges of an Sbc progenitor and that star formation ceased shortly after the tails were launched. We again use the models of Bruzual & Charlot (1993, 1995, private communication) for a Salpeter IMF over the mass range 0.1–125 $M_\odot$ and adopt an exponentially decreasing SFR with a time constant of 4 Gyr (typical of an Sbc galaxy; Bruzual & Charlot 1993) that is truncated after 10 Gyr and allowed to age another 500 Myr. This simulates the situation in which star formation within the disk is extinguished as the tail forms, and the ejected stellar population passively fades thereafter. While tidal tails frequently exhibit in situ star formation (e.g., Schweizer 1978; Mirabel, Lutz, & Maza 1991), it is usually not widespread. Under these assumptions, a population with a projected R-band surface brightness of 1 $L_{R,\odot}$ pc^{-2} should produce an ionizing flux of 2.36×10^4 photons s^{-1} cm^{-2}. Therefore equation (5) becomes $n_{\rm H\,I}^2 \alpha_B dL < 2.36 \times 10^4$ photons s^{-1} cm^{-2} Σ_R, which can be rewritten as follows:

$$\Sigma_R > 14.28\ L_{R,\odot}\ {\rm pc}^{-2}\left(\frac{N_{\rm H\,I}}{2\times 10^{20}\ {\rm cm}^{-2}}\right)^2\left(\frac{10\ {\rm kpc}}{dL}\right). \quad (7)$$

Noting that 1 $L_\odot$ pc^{-2} corresponds to $\mu R = 25.9$ mag arcsec^{-2}, we rewrite this as a condition on the surface brightness of the tidal features:

$$\mu_R < 23.0\ {\rm mag\ arcsec}^{-2} - 2.5\log\left[\left(\frac{N_{\rm H\,I}}{2\times 10^{20}\ {\rm cm}^{-2}}\right)^2\left(\frac{10\ {\rm kpc}}{dL}\right)\right]. \quad (8)$$

Referring to Figure 4c, we see that only the northern plume of Arp 220 is bright enough to ionize nearby tidal H I at the appropriate column densities. Neither the optical plume in the NGC 520 system nor the northern tail in the Arp 299 system appears bright enough to ionize the necessary columns of hydrogen unless the tidal features are unreasonably thick ($\sim$60 kpc). However, since we have no other explanation for the small-scale H I/optical differences illustrated in Figure 4c, we are hesitant to abandon this explanation too quickly.

A possible solution is to invoke continued star formation even after the tails are ejected. For instance, if we do not truncate the star formation rate after 10 Gyr, instead allowing the star formation rate to continue its exponential decline as the tail expands, then the ionizing flux per 1 $L_{R,\odot}$ pc^{-2} is 70 times higher than the value 2.36×10^4 photons s^{-1} cm^{-2} used above. This would lower the fiducial surface brightness in equation (8) from 23.0 mag arcsec^{-2} to 27.5 mag arcsec^{-2}, in which case the faint tidal features in NGC 520 ($\mu_R \sim 25$ mag arcsec^{-2}) and Arp 299 ($\mu_R \sim 26.5$ mag arcsec^{-2}) could indeed ionize the necessary column densities of adjoining H I.

The observed broadband colors of the tidal tails are not of sufficient quality to discriminate between these two star formation histories, since the expected color differences are only of order $B-R = 0.1$ mag. However, whether or not the gas is more highly ionized in the regions of interest can be addressed observationally. The expected emission measure (EM $= \int n_e^2\, dl$) can be parameterized as follows:

$$\mathrm{EM} = 0.42\ {\rm cm}^{-6}\ {\rm pc}\left(\frac{N_{\rm H\,I}}{2\times 10^{20}\ {\rm cm}^{-2}}\right)^2\left(\frac{10\ {\rm kpc}}{dL}\right)^2. \quad (9)$$

Since emission measures of order 0.2 cm^{-6} pc have been detected with modern CCD detectors (e.g., Donahue et al. 1995; Hoopes, Walterbos, & Rand 1999), there is some hope of being able to observationally determine if regions of the tidal tails are significantly ionized. If the gas has a clumpy distribution, then there should be some high-density peaks that might be sufficiently bright to yield reliable emission-line ratios. Such ratios would allow one to determine the nature of the ionizing source, e.g., photoionization versus shocks. Therefore, while we cannot assert unequivocally that photoionization plays a role in shaping the outer tidal morphologies, it is possible to test this hypothesis with future observations.

The hypothesis that ionizing flux from a stellar tidal feature may ionize gas in a nearby gaseous tidal feature is not necessarily at odds with the observation that many stellar tails are gas-rich. This is because tails with cospatial gas and stars arise from regions originally located within the stellar disk of the progenitors, while the optical faint gas-rich tidal features likely arise from regions beyond the optical disk (§ 3.1). In normal disk galaxies, the H I within the optical disk is dominated by a cooler component with a smaller scale height and velocity dispersion, while the H I beyond the optical disk is warmer and more diffuse, with a larger scale height and velocity dispersion (Braun 1995, 1997). As a result, dL should be considerably larger for purely gaseous tidal features than for optically bright tidal features.

4. CONCLUSIONS

In this paper we have described differences between gaseous and stellar tidal features. There are large-scale differences, such as extensive purely gaseous tidal features (the outer disks in NGC 520 and Arp 220 and the outer filament in Arp 299) and largely gas-poor optical features (tidal plumes in NGC 520 and Arp 220 and the inner filament in Arp 299). There are also smaller scale differences: the anticorrelation between the edges of gaseous and optical features depicted in Figure 4. A similar anticorrelation is observed between H I and optical shells in shell galaxies (Schiminovich et al. 1994, 1995; Schiminovich, van Gorkom, & van der Hulst 2000), many of which are believed to be more evolved merger remnants.

We have examined a number of possible explanations for these observations, including dust obscuration, differences in the original distribution of gas and starlight in the progenitor disks, gas cloud collisions within the developing tails, ram pressure stripping due to an extensive hot halo or an expanding superwind, and photoionization by either the central starburst or evolved sources in the tidal tails themselves. However, no single model easily and completely explains the observations, and it is conceivable that all explanations are playing a role at some level.

The most likely explanation for the lack of starlight associated with the outer tidal H I is that such features arise from the H I–rich but optically faint outer radii of the progenitor disks. The relatively short lifetimes of luminous stars and the large velocity dispersions of less luminous stars, especially with respect to the gas, will further dilute the luminous content of this material, and the H I–to–light ratio of the resulting tidal features will increase with time (Hibbard et al. 1994). Gaseous tidal extensions with very little detectable starlight would seem to be the natural consequence. The outer H I rings in NGC 520 and Arp 220 and the gas-rich outer filament in Arp 299 are all likely to arise from these gas-rich regions of their progenitor disks.

For the gas-poor tidal features, we suggest that the starburst has played an important role in shaping the gaseous morphology, either by sweeping the features clear of gas via a high-pressure expanding superwind or by excavating a clear sightline toward the starburst and allowing ionizing photons to penetrate the tidal regions. The primary supporting evidence for this conclusion is rather circumstantial: the five galaxies with the most striking H I/optical displacements (the three systems currently under study here and the H I accreting starburst systems M82 and NGC 4631) host massive nuclear starbursts with associated powerful outflows or superwinds aligned with the direction of the most extreme H I/optical displacements.

NGC 520, Arp 299, and Arp 220 each experienced prograde/polar or prograde/retrograde encounters. This relative geometry may be a prerequisite for the morphological differences reported here. Retrograde and polar encounters do not raise extensive tidal tails (e.g., Barnes 1988), leaving large gaseous disks in the inner regions. These disks should help collimate and "mass load" the superwind (Heckman et al. 1993; Suchkov et al. 1996), which in turn leads to denser and longer-lived winds. Simultaneously, the combination of opposite spin geometries provides the opportunity for the tidal tail from the prograde system to rise above the starburst region in the polar or retrograde system, where it may intersect the escaping superwind or UV radiation. If this suggestion is correct, only a system hosting a galactic superwind and experiencing a high-inclination encounter geometry should exhibit such extreme differences between its H I and optical tidal morphologies.

The observations do not allow us to discriminate between either the RPS or the photoionization models: simple calculations suggest that either is capable of affecting the diffuse outer gas if the geometry is right. There might be some evidence for an impinging wind on the outer material in Arp 299 from the increased velocity dispersion at several points (HY99); however, NGC 520 and Arp 220 show no such signatures. Photoionization is an attractive solution, as it offers a means of explaining the lack of tidal H I found at the base of otherwise gas-rich tidal tails in mergers that show no evidence of superwinds (e.g., NGC 7252, Arp 105, NGC 4039; see § 3.5.1).

Since any ionized hydrogen will emit recombination lines, both explanations can be checked observationally. The expected emission measure is given by equation (9), which predicts detectable features at the column densities of interest. The morphology of the ionized gas should reveal the nature of the ionizing source: photoionized gas should be smoothly distributed, while gas excited by RPS should be concentrated in dense shocked regions on the edges of the H I that are being compressed by the superwind, i.e., on the edges nearest the wind axis in Figures 1*d*, 2*d*, and 3*d*. If the gas is clumpy, there may be regions bright enough to allow line ratios to be measured, which should further aid in discriminating between photoionization and shock excitation.

Only two scenarios are offered to explain the small-scale anticorrelations: dust obscuration and photoionization due to evolved sources in the optical tails. Dust obscuration likely affects the apparent tidal morphologies at the lowest light levels, but we suspect that the dust content is too low to obscure the brighter tidal features significantly. However, if the tidal tails are highly ionized, with the neutral gas representing only a small fraction of the total hydrogen column density, it is possible that we are grossly underestimating the expected amount of absorption. This question can be investigated directly with submillimeter imaging of the cold dust in tidal tails.

The other possibility is that the UV flux from evolved sources in the optical tails is responsible for ionizing nearby diffuse outer H I. A simple calculation suggests that the tidal tail in Arp 220 is bright enough to ionize nearby H I, but the expected ionization flux from the optical tails in NGC 520 and Arp 299 is too low to explain the observed differences unless significant star formation continued within these features after their tidal ejection. If this is indeed the case, then the regions where the neutral gas column density drops rapidly (see Fig. 4) should contain ionized gas, which would emit recombination radiation. The expected levels of emission should be observable with deep-imaging techniques (see above). This situation requires that the gas and stellar features are physically close, not just close in projection, which can be tested with detailed numerical simulations.

We would like to thank L. Armus and T. Heckman for sharing unpublished results and R. Evans, J. van Gorkom, D. Schiminovich, and J. Barnes for useful discussions. We thank the referee, C. Mihos, for a thorough and useful report.

REFERENCES

Aaronson, M., Huchra, J., Mould, J., Schechter, P. L., & Tully, R. B. 1982, ApJ, 258, 64
Alton, P. B., et al. 1998, A&A, 335, 807
Appleton, P. N., Charmandaris, V., & Struck, C. 1996, ApJ, 468, 532
Appleton, P. N., Davies, R. D., & Stephenson, R. J. 1981, MNRAS, 195, 327
Appleton, P. N., Ghigo, F. D., van Gorkom, J. H., Schombert, J. M., & Struck-Marcell, C. 1987, Nature, 330, 140
Armus, L., Heckman, T. M., & Miley, G. K. 1990, ApJ, 364, 471
Barnes, J. E. 1988, ApJ, 331, 699
Barnes, J. E. 1992, ApJ, 393, 484
Barnes, J. E., & Hernquist, L. 1991, ApJ, 370, L65
———. 1996, ApJ, 471, 115
Bohlin, R. C., Savage, B. D., & Drake, J. F. 1978, ApJ, 224, 132
Braun, R. 1995, A&AS, 114, 409
———. 1997, ApJ, 484, 637
Bruzual, A. G., & Charlot, S. 1993, ApJ, 405, 538
Chevalier, R. A., & Clegg, A. W. 1985, Nature, 317, 44
Combes, F. 1978, A&A, 65, 47
Combes, F., Dupraz, C., Casoli, F., & Pagani, L. 1988, A&A, 203, L9

Condon, J. J., Helou, G., Sanders, D. B., & Soifer, B. T. 1990, ApJS, 73, 359
Corbelli, E., & Salpeter, E. E. 1993, ApJ, 419, 104
Corbelli, E., Schneider, S. E., & Salpeter, E. E. 1989, AJ, 97, 390
Dahlem, M., Heckman, T. M., Fabbiano, G., Lehnert, M. D., & Gilmore, D. 1996, ApJ, 461, 724
Donahue, M., Aldering, G., & Stocke, J. T. 1995, ApJ, 450, L45
Dove, J. B., & Shull, J. M. 1994, ApJ, 423, 196
Dove, J. B., Shull, J. M., & Ferrara, A. 2000, ApJ, in press (astro-ph/9903331)
Downes, D., & Solomon, P. M. 1998, ApJ, 507, 615
Duc, P.-A., Brinks, E., Wink, J. E., & Mirabel, I. F. 1997, A&A, 326, 537
English, J., et al. 2000, AJ, submitted
Felton, J. E., & Bergeron, J. 1969, ApJ, 4, L155
Filippenko, A. V., & Sargent, W. L. W. 1992, AJ, 103, 28
Gardiner, L. T., & Noguchi, M. 1996, MNRAS, 278, 191
Gunn, J. E., & Gott, J. R. 1972, ApJ, 176, 1
Heckman, T. M., Armus, L., & Miley, G. K. 1987, AJ, 93, 276
———. 1990, ApJS, 74, 833 (HAM90)
Heckman, T. M., Armus, L., Weaver, K. A., & Wang, J. 1999, ApJ, 517, 130
Heckman, T. M., Dahlem, M., Eales, S. A., Fabbiano, G., & Weaver, K. 1996, ApJ, 457, 616
Heckman, T. M., Lehnert, M., & Armus, L. 1993, in The Evolution of Galaxies and Their Environment, ed. H. A. Thronson & J. M. Shull (Dordrecht: Kluwer), 455
Hibbard, J. E. 1995, Ph.D. thesis, Columbia Univ.
Hibbard, J. E., Guhathakurta, P., van Gorkom, J. H., & Schweizer, F. 1994, AJ, 107, 67
Hibbard, J. E., & Mihos, J. C. 1995, AJ, 110, 140
Hibbard, J. E., van der Hulst, J. M., & Barnes, J. E. 2000, in preparation
Hibbard, J. E., & van Gorkom, J. H. 1996, AJ, 111, 655 (HvG96)
Hibbard, J. E., & Yun, M. S. 1996, in Cold Gas at High Redshift, ed. M. Bremer, H. Rottgering, P. van der Werf, & C. L. Carilli (Dordrecht: Kluwer), 47
———. 1999, AJ, 118, 162 (HY99)
———. 2000, in preparation
Hilker, M., & Kissler-Patig, M. 1996, A&A, 314, 357
Hill, J. K. 1974, A&A, 34, 431
Hoffman, L. G., Lu, N. Y., Salpeter, E. E., Farhat, B., Lamphier, C., & Roos, T. 1993, AJ, 106, 39
Hoopes, C., Walterbos, R., & Rand, R. 1999, ApJ, 522, 669
Irwin, J. A., Seaquist, E. R., Taylor, A. R., & Duric, N. 1987, ApJ, 313, L91
Joseph, R. D., & Wright, G. S. 1985, MNRAS, 214, 87
Lanzetta, K. M., Bowen, D. V., Tytler, D., & Webb, J. K. 1995, ApJ, 442, 538
Lehnert, M. D., & Heckman, T. M. 1996, ApJ, 462, 651
Leitherer, C., et al. 1999, ApJS, 123, 3
Lonsdale, C. J., Persson, S. E., & Matthews, K. 1984, ApJ, 287, 95
Maloney, P. 1993, ApJ, 414, 41
Meurer, G. R., Bicknell, G. V., & Gingold, R. A. 1985, Proc. Astron. Soc. Australia, 6, 195
Mihos, J. C. 2000, in preparation
Mihos, J. C., & Bothun, G. D. 1998, ApJ, 500, 619
Mihos, J. C., Bothun, G. D., & Richstone, D. O. 1993, ApJ, 418, 82
Mihos, J. C., & Hernquist, L. 1996, ApJ, 464, 641
Mirabel, I. F., Lutz, D., & Maza, J. 1991, A&A, 243, 367
Moore, B., & Davis, M. 1994, MNRAS, 270, 209
Noguchi, M. 1988, A&A, 201, 37
Nordgren, T. E., Chengalur, J. N., Salpeter, E. E., & Terzian, Y. 1997, AJ, 114, 77
Norman, C., Bowen, D. V., Heckman, T., Blades, C., & Danly, L. 1996, ApJ, 472, 73
O'Donnell, J. E. 1994, ApJ, 422, 1580
Pietz, J., Kerp, J., Kalberla, P. M. W., Burton, W. B., Hartmann, D., & Mebold, U. 1998, A&A, 332, 55
Sakamoto, K., Scoville, N. Z., Yun, M. S., Crosas, M., Genzel, R., & Tacconi, L. J. 1999, ApJ, 514, 68
Sanders, D. B., Scoville, N. Z., Sargent, A. I., & Soifer, B. T. 1988, ApJ, 324, L55
Sanders, D. B., Scoville, N. Z., & Soifer, B. T. 1991, ApJ, 370, 158
Schiminovich, D., van Gorkom, J. H., & van der Hulst, J. M. 2000, AJ, submitted
Schiminovich, D., van Gorkom, J. H., van der Hulst, J. M., & Kasow, S. 1994, ApJ, 423, L101
Schiminovich, D., van Gorkom, J. H., van der Hulst, J. M., & Malin, D. F. 1995, ApJ, 444, L77
Schlegel, D. J., Finkbeiner, D. P., & Davis, M. 1998, ApJ, 500, 525
Schombert, J. M., Wallin, J. F., & Struck-Marcell, C. 1990, AJ, 99, 497
Schweizer, F. 1978, in IAU Symp. 77, The Structure and Properties of Nearby Galaxies, ed. E. M. Berkhuijsen & R. Wielebinski (Dordrecht: Reidel), 279
Scoville, N. Z., Yun, M. S., & Bryant, P. M. 1997, ApJ, 484, 702
Shopbell, P. L., & Bland-Hawthorn, J. 1998, ApJ, 493, 129
Simkin, S. M., van Gorkom, J. H., Hibbard, J. E., & Hong-Jun, S. 1987, Science, 235, 1367
Smith, B. J. 1994, AJ, 107, 1695
Smith, B. J., Struck, C., & Pogge, R. W. 1997, ApJ, 483, 754
Sofue, Y. 1994, ApJ, 423, 207
Sofue, Y., & Wakamatsu, K. 1993, A&A, 273, 79
Soifer, B. T., et al. 1984, ApJ, 283, L1
Spitzer, L. 1956, ApJ, 124, 20
Stanford, S. A., & Balcells, M. 1991, ApJ, 370, 118
Stockton, A. 1974a, ApJ, 187, 219
———. 1974b, ApJ, 190, L47
Stockton, A., & Bertola, F. 1980, ApJ, 235, 37
Strickland, D. K., Ponman, T. J., & Stevens, I. R. 1997, A&A, 320, 378
Struck, C. 1997, ApJS, 113, 269
Struck-Marcell, C. 1990, AJ, 99, 71
Suchkov, A. A., Balsara, D. S., Heckman, T. M., & Leitherer, C. 1994, ApJ, 430, 511
Suchkov, A. A., Berman, V. G., Heckman, T. M., & Balsara, D. S. 1996, ApJ, 463, 528
Toomre, A., & Toomre, J. 1972, ApJ, 178, 623
van der Hulst, J. M. 1979, A&A, 75, 97
van Gorkom, J. H. 1993, in The Evolution of Galaxies and Their Environment, ed. H. A. Thronson & J. M. Shull (Dordrecht: Kluwer), 345
Vogler, A., & Pietsch, W. 1996, A&A, 311, 35
Wallin, J. F. 1990, AJ, 100, 1477
Wang, B. 1995, ApJ, 444, 590
Wang, Q. D., Walterbros, R. A. M., Steakley, M. F., Norman, C. A., & Braun, R. 1995, ApJ, 439, 176
Weil, M. L., & Hernquist, L. 1993, ApJ, 405, 142
Weliachew, L., Sancisi, R., & Guelin, M. 1978, A&A, 65, 37
Wevers, B. H. M. R., Appleton, P. N., Davies, R. D., & Hart, L. 1984, A&A, 140, 125
Yun, M. S. 1992, Ph.D. thesis, Harvard Univ.
———. 1999, in IAU Symp. 186, Galaxy Interactions at Low and High Redshift, ed. D. Sanders & J. Barnes (Dordrecht: Kluwer), 8
Yun, M. S., & Hibbard, J. E. 2000a, in preparation
———. 2000b, ApJ, submitted
Yun, M. S., Ho, P. T. P., & Lo, K. Y. 1993, ApJ, 411, L17
———. 1994, Nature, 372, 530